Turkish Journal of Electrical Engineering & Computer Sciences
http://journals.tubitak.gov.tr/elektrik/
Research Article
Turk J Elec Eng & Comp Sci
(2018) 26: 1736 – 1746
© TÜBİTAK
doi:10.3906/elk-1801-127

Compact microstrip lowpass filter with ultrasharp response using a square-loaded modified T-shaped resonator

Ali PIRASTEH, Saeed ROSHANI*, Sobhan ROSHANI
Department of Electrical Engineering, Kermanshah Branch, Islamic Azad University, Kermanshah, Iran

Received: 13.01.2018 • **Accepted/Published Online:** 06.04.2018 • **Final Version:** 27.07.2018

Abstract: A miniaturized lowpass filter (LPF) with ultrasharp response, good figure of merit (FOM), and simple structure is proposed. The designed structure is fabricated and measured with a 2.9 GHz cut-off frequency. The proposed LPF consists of high impedance lines that are loaded by three similar resonators and two uniform suppressing cells. The filter size is only 0.08 × 0.23 λg, which indicates small circuit size. The proposed design exhibits good features, such as an ultrasharp roll-off rate of about 1609 dB/GHz and a good FOM of 162,820. The insertion loss of the proposed LPF is less than 0.14 dB in the passband. With these excellent obtained specifications and flat group delay, this structure can be used in wireless antennae.

Key words: Microstrip, low-pass filters (LPF), sharp roll-off, resonator

1. Introduction

Microstrip low-pass filters (LPFs) are important passive elements for the attenuation of unwanted signals and noise in communication systems [1]. LPFs are widely used to suppress unwanted harmonics in active and passive devices such as power dividers, couplers [2–4], and amplifiers [5,6]. Therefore, several studies have been reported recently to improve LPF parameters, with various structures and methods to move these parameters closer to the ideal values. The ideal parameters for a LPF are zero insertion loss and highly attenuated return loss in the pass band, a sharp roll-off rate in the transition band, compact circuit size, and an ultrawide stopband [7].

In [8,9], two LPFs with an ultrawide stopband were reported. Unfortunately, these filters are large and have complicated structures. In [10–13], small LPFs were designed, but all of these reported works suffer from low sharpness and relatively complex structure. In [14,15], sharp LPFs were reported, but these reported structures are not able to solve the large dimensions problem. In [16–19], compact LPFs with sharp responses were introduced. However, in all of the above-mentioned structures, size reduction and an ultrasharp transition band were not achieved. Therefore, the FOM parameters for the reported structures are not superior.

In this article, a compact LPF with a simple structure is proposed, which has good features, such as ultrasharp roll-off rate, low insertion loss in the passband, very compact size, and high FOM.

2. Design procedure of the proposed LPF

The proposed microstrip LPF consists of three similar resonators and two uniform suppressing cells. A primitive T-shaped resonator is used as the building block of the main resonator. The primitive T-shaped resonator

*Correspondence: s_roshany@yahoo.com

structure is shown in Figure 1a, while Figure 1b shows the LC equivalent circuit of the primitive T-shaped resonator.

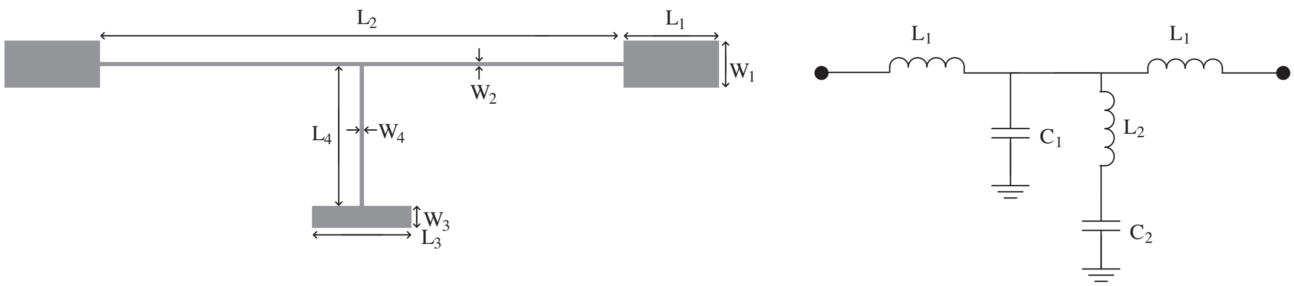

(a) (b)

Figure 1. (a) A primitive T-shaped resonator. (b) LC equivalent circuit of primitive T-shaped resonator.

The dimensions of the primitive T-shaped resonator are: W_1=1.6, W_2 = W_4 = 0.1, W_3 = 0.75, L_1= 3, L_2 = 16.56, L_3= 3.15, and L_4= 4.75 mm.

The values of the inductors and capacitors used in Figure 1b are: L_1 = 5.64 nH, L_2= 5.58 nH, C_1 = 0.4 pF, and C_2= 0.142 pF. The transfer function of the LC equivalent circuit with resistance matching of (R) in a primitive T-shaped resonator can be obtained from the following equation:

$$\frac{V_{out}}{V_{in}} = \frac{2\,R + M\,S^2}{2\,R + A\,S + B\,S^2 + C\,S^3 + D\,S^4 + E\,S^5}, \quad (1)$$

where

$$M = 2RC_2L_3,$$

$$A = 2L_1 + R^2(C_1 + C_2),$$

$$B = 2R(L_1C_1 + L_1C_2 + L_2C_2),$$

$$C = L_1^2C_1 + L_1^2C_2 + 2L_1L_2C_2 + R^2C_1L_2C_2,$$

$$D = 2RL_1C_1L_2C_2 \text{ and}$$

$$E = L_1^2C_1L_2C_2.$$

Transmission zero frequency of the primitive T-shaped resonator is

$$f_z = \frac{1}{2\,\pi\sqrt{L_2\,C_2}} \quad (2)$$

The simulation response of the S_{21} parameter, as a function of the L_3 parameter for the primitive T-shaped resonator, is shown in Figure 2a. Figure 2b shows EM and LC equivalent circuit simulation results for primitive T-shaped resonator. As the results show, the primitive T-shaped resonator creates a transmission zero. Adjusting the value of L_3 leads to a change in the location of this transmission zero. Increasing the length of L_3 decreases the obtained frequency of the stopband. The roll-off rate of the primitive T-shaped resonator is 22.38 dB/GHz.

As seen in Figure 2a, the insertion loss parameter of the primitive T-shaped resonator is undesirable. The modified T-shaped resonator (MTR) is introduced in order to reduce the insertion loss and improve sharpness of the primitive resonator, as shown in Figure 3a. Figure 3b shows the LC equivalent circuit of the MTR.

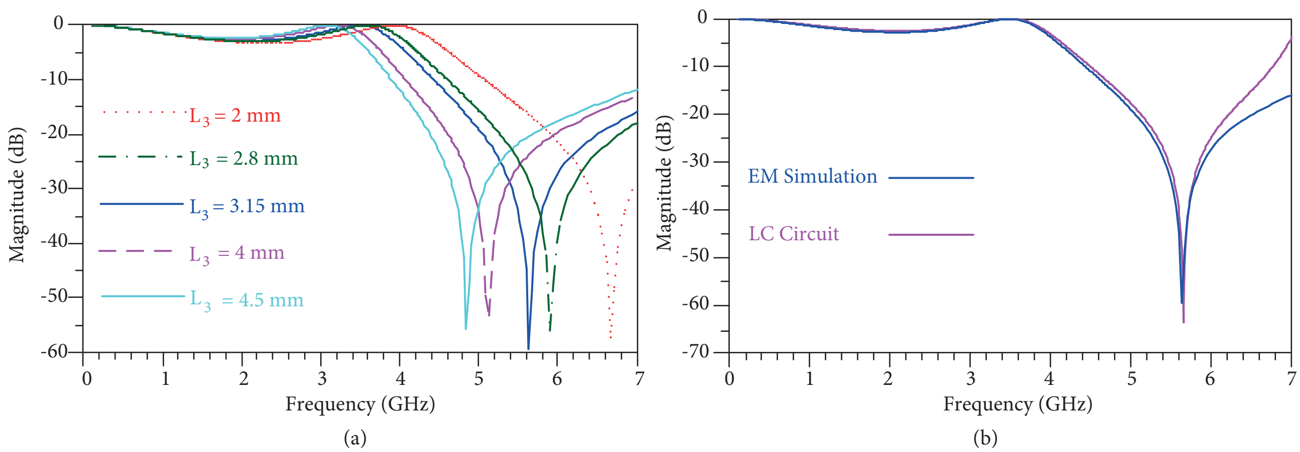

Figure 2. (a) Simulation results of S_{21} for primitive T-shaped resonator. (b) EM and LC equivalent circuit simulation results for primitive T-shaped resonator.

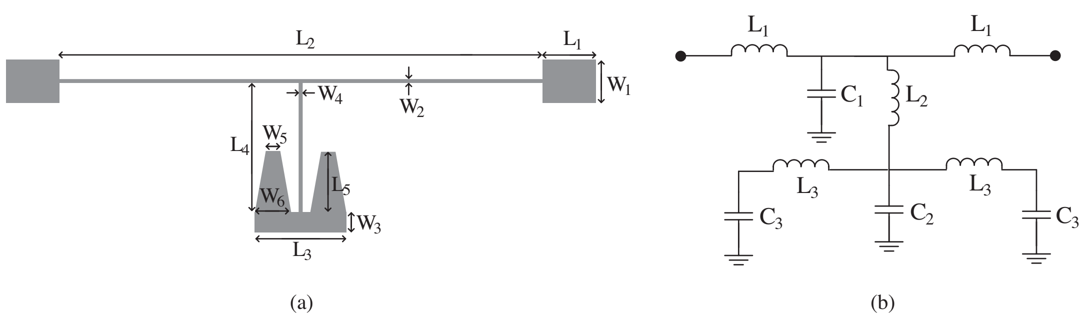

Figure 3. (a) Modified T-shaped resonator (MTR). (b) LC equivalent circuit of MTR.

The dimensions of the MTR cell are: $W_5 = 0.5$, $W_6 = 1.25$, $L_5 = 2.25$ mm. The values of the LC equivalent circuit elements in Figure 3b are as follows: $L_1 = 4.6$ nH, $L_2 = 2.8$ nH, $L_3 = 0.44$ nH, $C_1 = 0.35$ pF, $C_2 = 0.3$ pF, and $C_3 = 0.126$ pF.

As shown in Figure 4a, the MTR performance is better than the primitive resonator and the insertion loss is partly improved. The MTR cell has a sharper transition band than the primitive T-shaped resonator, and the location of the transmission zero is moved to the lower frequencies. Figure 4b shows EM and LC equivalent circuit simulations for the MTR. The roll-off rate for the MTR cell is 36.7 dB/GHz, which shows that its transition band is sharper than the primitive T-shaped resonator. In the next step, a square-loaded modified T-shaped resonator (SLMTR) is proposed, as shown in Figure 5a, to increase sharpness and improve the insertion loss parameter. The dimensions of the SLMTR are: $W_7 = L_7 = 1$, $L_6 = 1.4$, and $W_8 = 0.1$ mm. Figure 5b shows the LC equivalent circuit for the SLMTR. The values of SLMTR elements are as follows: $L_1 = 5.41$ nH, $L_2 = 2.15$ nH, $L_3 = 0.53$ nH, $L_4 = 0.25$ nH, $C_1 = 0.07$ pF, $C_4 = C_{gap} = C_3 = 0.125$ pF, and $C_2 = 0.29$ pF. As shown in Figure 6a, the SLMTR cell has a better performance than the other two resonators. Figure 6b shows EM and LC equivalent circuit simulations for the SLMTR. The SLMTR structure improved sharpness in the transition band and moved the location of the transmission zero to the lower frequencies.

The main resonator is constructed by cascading three SLMTRs as shown in Figure 7. In the main resonator, the gap between each section is equal to $L_8 = 0.2$ mm. The main resonator shows an ultrasharp response, as shown in Figure 8. The roll-off rate of the main resonator is 711.53 dB/GHz, which shows a

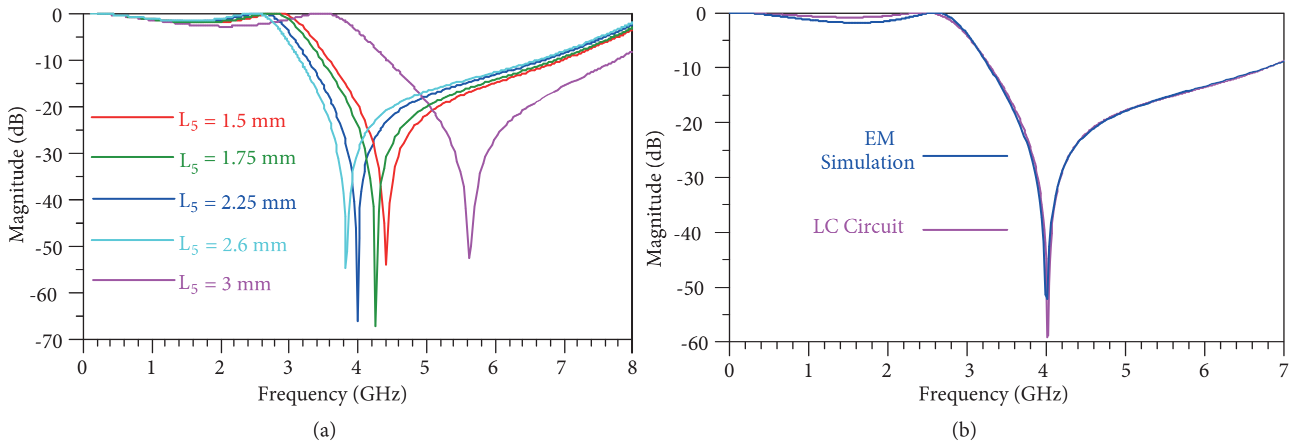

Figure 4. (a) Simulation results of S_{21} for MTR. (b) EM and LC equivalent circuit simulations for MTR.

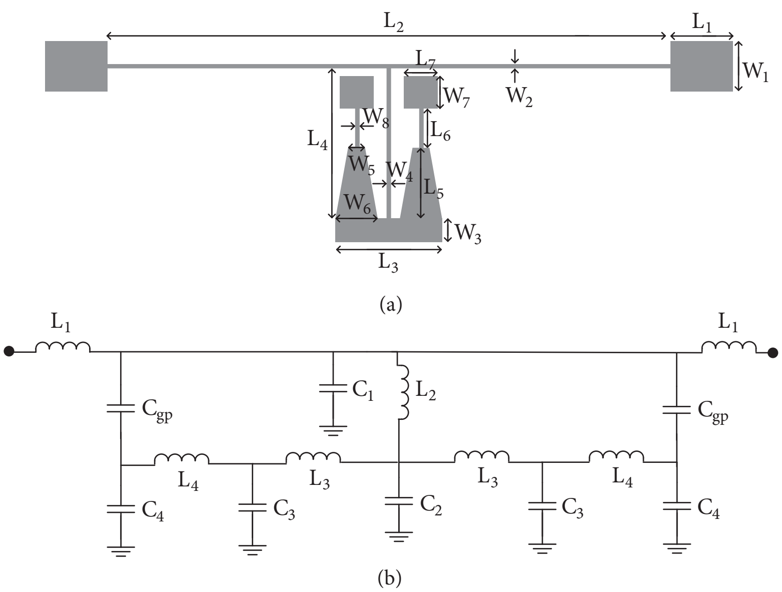

Figure 5. (a) Square-loaded MTR (SLMTR). (b) LC equivalent circuit of SLMTR.

674.83 dB/GHz sharper transition band than the MTR cell. Unfortunately, despite the sharp response of the main resonator, the insertion loss parameter is not so good. In order to have a better performance and to reduce the insertion loss in the passband, two suppressing cells are adopted, as depicted in Figure 9a. The suppressing cells dimensions are as follows: $W_9 = W_{10} = W_{11} = W_{12} = W_{13} = W_{14} = W_{17} = W_{18} = W_{19} = W_{20} = 0.1$, $L_{27} = L_{28} = 1.52$, $L_{21} = L_{22} = 4.75$, $L_9 = L_{11} = L_{13} = 2$, $L_{10} = L_{12} = L_{14} = 3$, $L_{17} = L_{20} = 2.25$, $L_{18} = L_{19} = 2.65$, $L_{15} = 3.5$, $L_{16} = 2.5$, $L_{29} = L_{30} = 3.15$, $W_{15} = W_{16} = 0.75$, $L_{24} = L_{25} = 0.3$, and $L_{23} = L_{26} = 0.2$ mm. Figure 9b shows the LC equivalent circuit for the suppressing cells of the proposed LPF. The elements values for LC equivalent circuit of the suppressing cells are as follows: $L_1 = 0.15$ nH, $L_2 = 1.89$ nH, $L_3 = 0.243$ nH, $L_4 = 0.25$ nH, $L_5 = 0.992$ nH, $L_6 = 0.25$ nH, $L_7 = 3.35$ nH, $C_1 = 0.18$ pF, $C_2 = C_4 = 0.1$ pF, $C_3 = 0.112$ pF, $C_5 = 0.162$ pF, $C_6 = 0.122$ pF, $C_{gp_1} = 0.15$ pF, and $C_{gp_2} = 1.25$ pF. The frequency response of suppressing cells is depicted and in Figure 10a. Figure 10b shows EM and LC equivalent circuit simulations for suppressing cells.

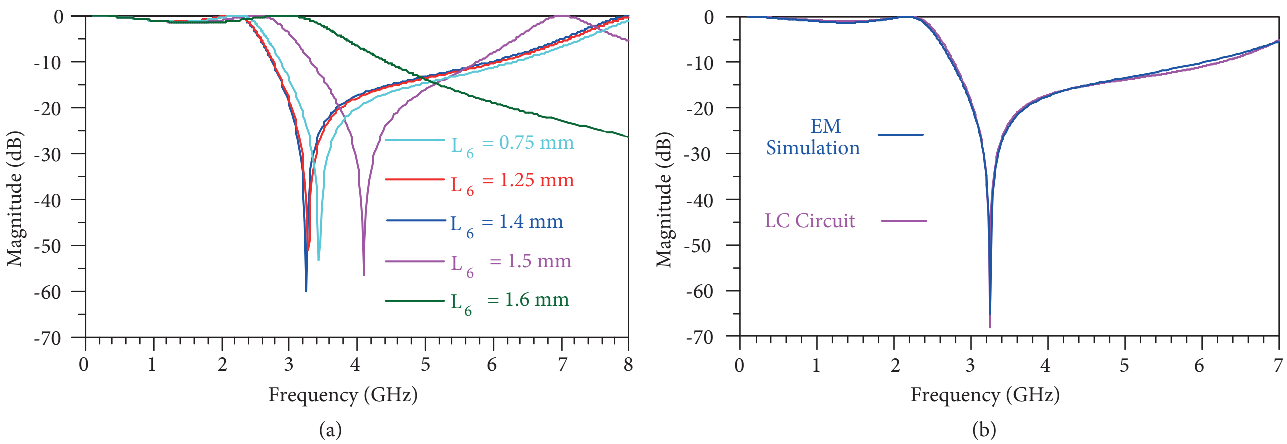

Figure 6. (a) SLMTR S_{21} simulation result. (b) EM and LC equivalent circuit simulations for SLMTR.

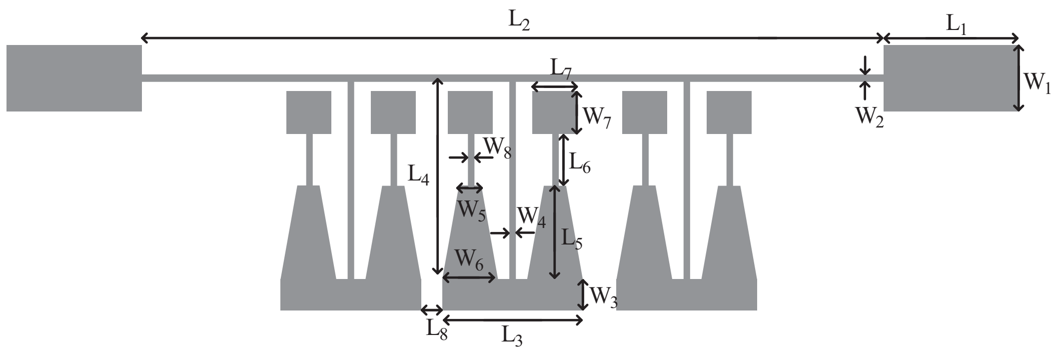

Figure 7. The layout of the main resonator.

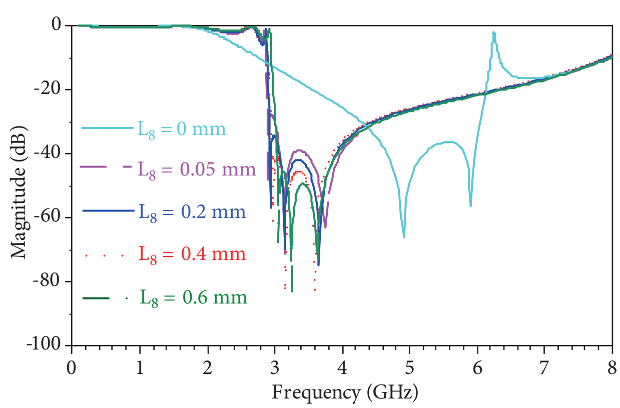

Figure 8. S_{21} simulation results for the main resonator.

The proposed LPF is constructed by combining the main resonator and suppressing cells. The layout structure and fabricated photo of the proposed LPF are depicted in Figures 11 and 12, respectively. The proposed microstrip LPF is fabricated on reinforced Teflon (RT)/Duroid 5880 substrate (ε_r = 2.2, h = 0.508 mm, and loss tangent of 0.0009) (DuPont, Wilmington, DE, USA). The overall size of the proposed LPF is 16.56 $\times$ 5.6 mm^2 (0.08 $\times$ 0.23 λg, where, λg is the guided wavelength at 2.9 GHz).

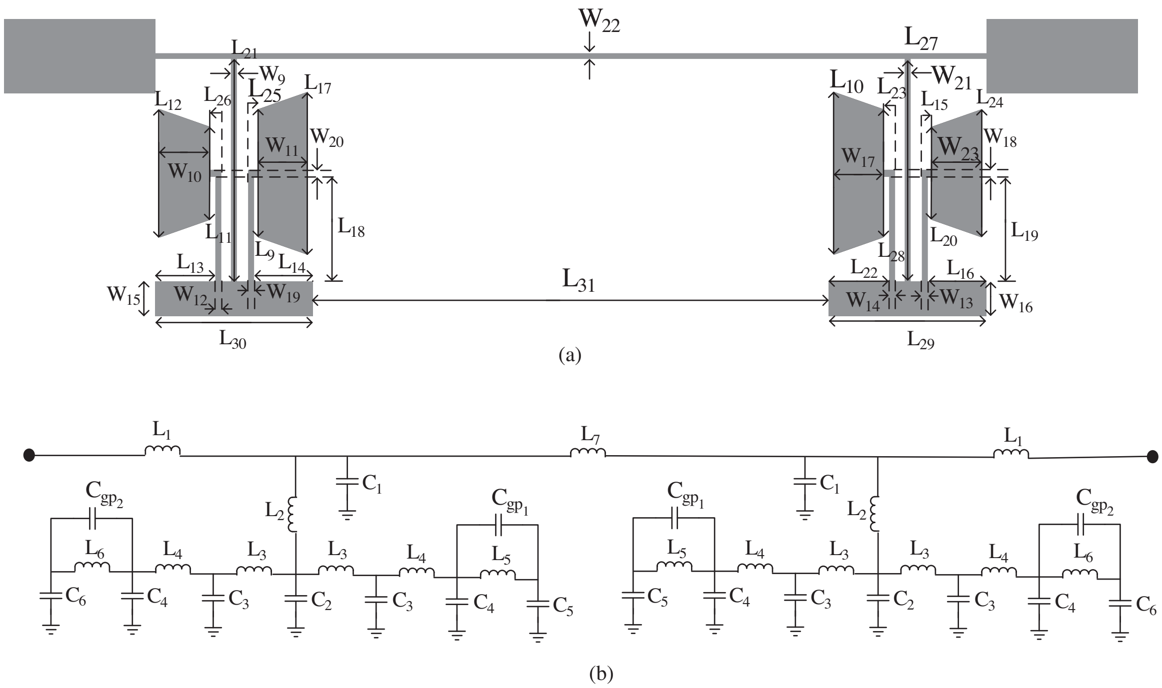

Figure 9. (a) Suppressing cells of the proposed LPF. (b) LC equivalent circuit for the suppressing cells of the proposed LPF.

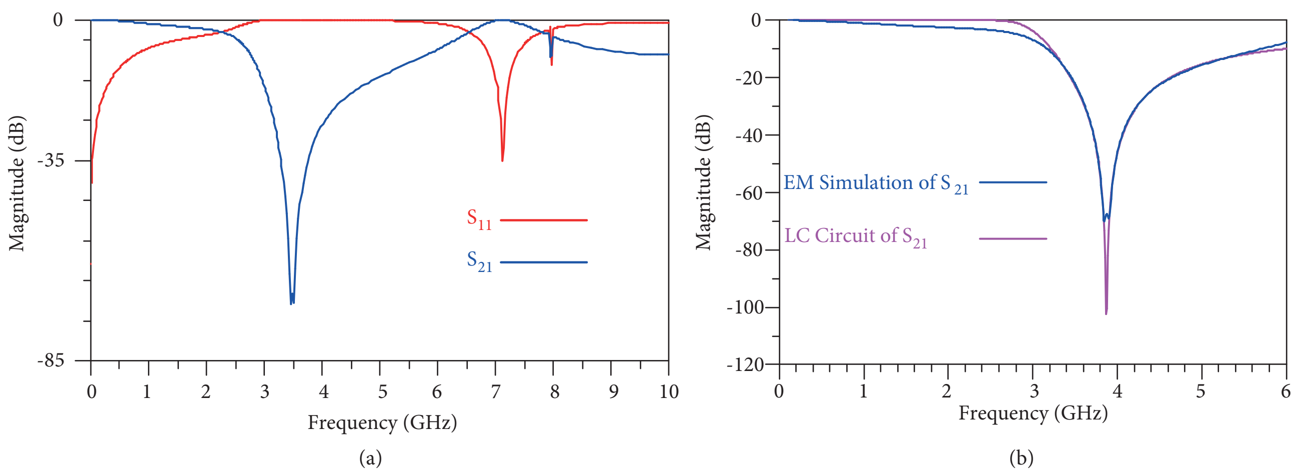

Figure 10. (a) Frequency response of the suppressing cells. (b) EM and LC equivalent circuit simulations for suppressing cells.

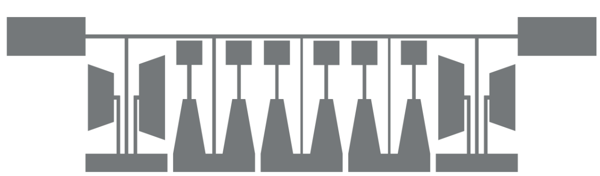

Figure 11. Layout of the proposed LPF.

3. Measured and simulated results

The proposed LPF was measured with HP8720B network analyzer (Agilent, Santa Clara, CA, USA). The measurement workbench is shown in Figure 13. Advanced Design System (Agilent) was used for simulation, and the HP8720B network analyzer was used for S-parameters measurements.

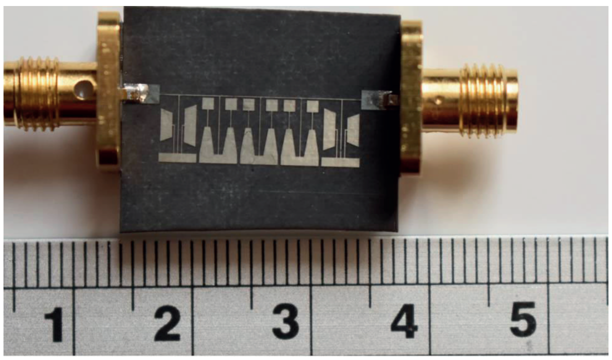

Figure 12. Fabricated photo of the proposed LPF.

Figure 13. The measurement workbench with an HP8720B network analyzer.

The simulated and measured frequency responses of the fabricated LPF are shown in Figure 14.

As seen in Figure 14, the measured and simulated results of the LPF are in good agreement. The results show an ultrasharp transition band with low insertion loss in the passband.

The measured and simulated insertion loss of the proposed LPF in the passband is depicted in Figure 15. The simulated insertion loss in the passband is 0.14 dB and the measured value of this parameter in the passband is 0.2 dB according to the network analyzer.

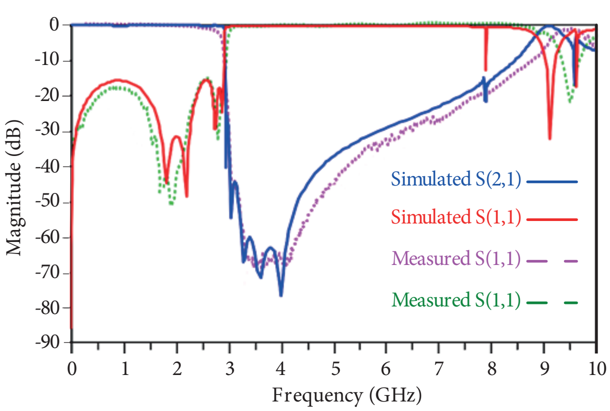

Figure 14. Frequency responses of the proposed LPF.

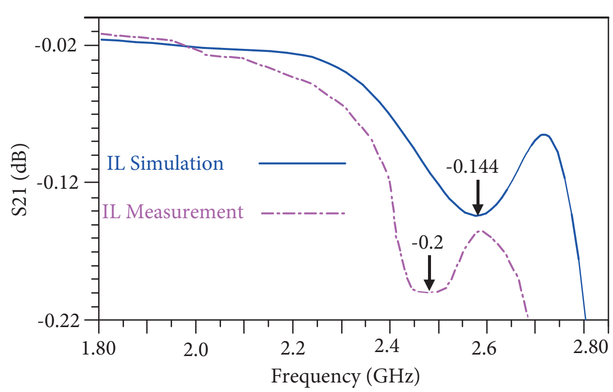

Figure 15. Insertion loss of the proposed LPF in the pass band.

The measured S-parameters of the proposed LPF with HP8720B network analyzer are shown in Figure 16.

The simulated group delay of presented LPF in passband is shown in Figure 17. The group delay of

(a) (b)

Figure 16. The measured S-parameters of the proposed LPF with an HP8720B network analyzer. (a) S11 and (b) S21.

presented LPF is very flat because the maximum mutability in the proposed LPF at 55% passband is only 0.04 ns.

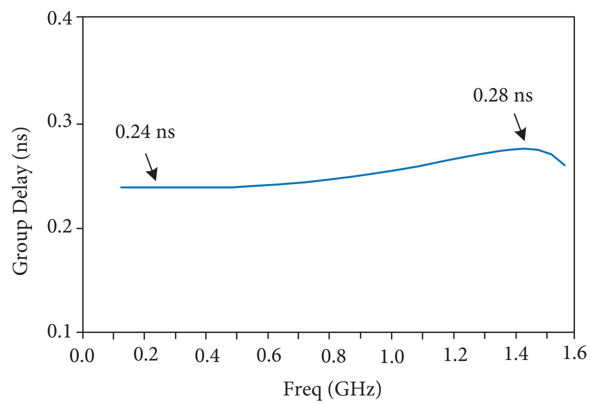

Figure 17. Group delay in the passband of the proposed LPF.

Comparisons between the designed LPF performance and similar reported structures [14–27] are shown in the Table. In this table, the sharpness of transition band is calculated as follows [13]:

$$\xi = \frac{\alpha_{max} - \alpha_{min}}{f_s - f_c} (dB/GHz), \tag{3}$$

where f_s is –40 dB stop-band frequency and f_c is the –3 dB cut-off frequency. The α_{max} and α_{min} parameters are –40 dB and –3 dB attenuation points, respectively. In the proposed design, the corresponding frequencies of f_S and f_C are 2.932 GHz and 2.912 GHz, which results in a sharpness of 1608.69. The proposed LPF shows the sharpest transition band compared to the other related works.

The relative stopband bandwidth parameter in Table is calculated as follows:

$$RSB = \frac{\text{stop band } (-25dB)}{\text{stopband center frequency}} \tag{4}$$

Table. Performance comparison between the designed LPF and similar reported works.

Refs	ζ	RSB	SF	NCS	AF	FOM
[14]	84.69	1.51	2	0.143 × 0.156	1	11,625
[15]	217	1.65	2	0.290 × 0.124	1	19,931
[16]	84	0.67	1.5	0.317 × 0.270	1	987
[17]	178.9	1.73	2	0.168 × 0.138	1	26,912
[18]	92.5	1.35	3	0.351 × 0.106	1	10,106
[19]	189	0.90	2	0.200 × 0.180	1	4724
[20]	129	1.62	2	0.730 × 0.130	1	4430
[21]	78	1.7	2	0.160 × 0.100	2	8287
[22]	57.8	1.61	3.2	0.120 × 0.100	1	27,142
[23]	94	1.26	2.3	0.244 × 0.169	1	6616
[24]	104	1.8	2.5	0.189 × 0.121	1	20,526
[25]	112	1.674	2	0.110 × 0.100	1	34,088
[26]	206.51	1.66	2.2	0.020	1	36,969
[27]	411	2.8	1.0	0.158 × 0.128	1	57,073
Proposed work	1608.69	0.77	2.5	0.080 × 0.230	1	162,820

The normalized circuit size parameter in the Table is defined as follows:

$$NCS = \frac{\text{physical filter size (length } \times \text{ width)}}{\lambda_g^2}, \tag{5}$$

where λg is defined as the guided wavelength at f_c (–3 dB cut-off frequency). As the results show, the proposed filter demonstrates the smallest size compared to the other reported works in this comparison.

The suppression factor in the Table is

$$SF = \frac{\text{rejection level in stopband}}{10} \tag{6}$$

The architecture factor parameter in the Table is considered 1. When the structure is in two dimensions, this parameter should be considered 2, and when the structure is in three dimensions, this parameter should be assumed 3.

The FOM in the Table is

$$FOM = \frac{\xi \times RSB \times SF}{NCS \times AF} \tag{7}$$

In this comparison, the designed LPF has the highest FOM among the other reported works.

4. Conclusion

A novel, ultrasharp, and very compact LPF with a simple structure is proposed in this paper. The proposed filter is composed of three similar resonators and two suppressing cells. The proposed LPF was designed, fabricated, and measured. With these good features, such as an ultrasharp response of 1608.69, compact circuit size of 0.08 × 0.23 λg, and very high FOM of about 162,820, the designed LPF can be used in modern communication and microwave circuits.

References

[1] Hong JS, Lancaster MJ. Microstrip Filters for RF/Microwave Applications. New York, NY, USA: Wiley, 2004.

[2] Hayati M, Roshani S, Roshani S. Miniaturized Wilkinson power divider with nth harmonic suppression using front coupled tapered CMRC. Appl Comput Electrom 2013; 28: 221-227.

[3] Roshani S, Siahkamari P, Siahkamari H. Compact, harmonic suppressed Gysel power divider with plain structure. Frequenz 2017; 71: 221-226.

[4] Roshani S. A Wilkinson power divider with harmonics suppression and size reduction using meandered compact microstrip resonating cells. Frequenz 2017; 71: 517-522.

[5] Roshani S, Hayati M, Setayeshi S, Roshani S, Mohamadpour G. A miniaturized harmonic suppressed power amplifier integrated with lowpass filter for long term evolution application. Analog Integr Circ S 2016; 89: 197-204.

[6] Hayati M, Roshani S. A novel miniaturized power amplifier with nth harmonic suppression. AEU-Int J Electron C 2014; 68: 1016-1021.

[7] Mandal MK, Mondal P, Sanyal S, Chakrabarty A. Low insertion loss, sharp rejection and compact microstrip low pass-filters. IEEE Microw Wirel Co 2007; 16: 600-602.

[8] Ma K, Yeo K S. New ultra wide stopband low pass filter using transformed radial stubs. IEEE T Microw Theory 2011; 59: 604-611.

[9] Roshani S. A compact microstrip low-pass filter with ultra wide stopband using compact microstrip resonant cells. Int J Microw Wirel T 2017; 9: 1023-1027.

[10] Wei F, Chen L, Shi XW, Huang QL, Wang XH. Compact low pass filter with wide stop band using coupled line hairpin unit. Electron Lett 2010; 46: 88-90.

[11] Deng K, Xue Q, Che W. Improved compact microstrip resonance cell lowpass filter with wide stopband characteristics. Electron Lett 2007; 43: 463-464.

[12] Sheikhi A, Alipour A, Abdipour A. Design of compact wide stopband microstrip low pass filter using t-shaped resonator. IEEE Microw Wirel Co 2017; 27: 111-113.

[13] Kumar L, Parihar MS. Compact hexagonal shape elliptical low pass filter with wide stopband. IEEE Microw Wirel Co 2016; 26: 978-980.

[14] Hayati M, Gholami M, S Vaziri H, Zaree T. Design of microstrip low pass filter with wide stopband sharp roll off using hexangular shaped resonator. Electron Lett 2015; 51: 69-71.

[15] Karimi G, Lalbakhsh A, Siahkamari H. Design of sharp roll off low pass filter with ultra wide stop band. IEEE Microw Wirel Co 2013; 23: 303-305.

[16] Raphika PM, Abdulla P, Jasmine PM. Compact low pass filter with a sharp roll off using patch resonators. Microw Opt Techn Let 2014; 56: 2534-2536.

[17] Hayati M, Abdipour A, Abdipour Ar. Compact microstrip low pass filter with sharp roll off and ultra-wide stop band. Electron Lett 2013; 49: 1159-1160.

[18] Li JL, SW Qu, Quan X. Compact microstrip low pass filter with sharp roll-off and wide stop band. Electron Lett 2009; 45: 110-111.

[19] Xiao M, Sun G, Li X. A lowpass filter with compact size and sharp roll off. IEEE Microw Wirel Co 2015; 25: 790-792.

[20] Zhang P, Li M, Wang J. Miniaturized lowpass filter with ultra-wide stopband using dual plan defected structures. IEICE Electron Expr 2014; 12: 1-7.

[21] Chen FC, Hu HT, Qiu JM, Chu QX. High-selectivity low-pass filters with ultra wide stopband based on defected ground structures. IEEE T Comp Pack Man 2015; 5: 1313-1319.

[22] Zhang B, Shaosheng L, Jianming H. Compact lowpass filter with wide stopband using coupled rhombic stubs. Electron Lett 2015; 51: 264-266.

[23] Raphika P, Abdulla P, Jasmine P. Planar elliptic function lowpass filter with sharp roll-off and wide stopband. Microw Opt Techn Let 2016; 58: 133-136.

[24] Jiang S, Xu J. Sharp roll-off planar lowpass filter with ultra-wide stopband up to 40 GHz. Electron Lett 2017; 53: 734-735.

[25] Roshani S, Golestanifar A, Ghaderi A, Roshani S. A miniaturized LPF with sharp transition-band using semi-circle resonators. Appl Comput Electrom 2017; 32: 344-351.

[26] Abdipour A, Abdipour AR, Lorestani F. A compact microstrip lowpass filter with sharp roll-off rate and ultra-wide stopband employing coupled polygon patches. Prog Electromagn Res-C 2017; 76: 171-183.

[27] Roshani S, Golestanifar A, Ghaderi A, Siahkamari H, Abbott D. High performance microstrip low pass filter for wireless communications. Wireless Pers Commun 2018; 99: 497-507.